

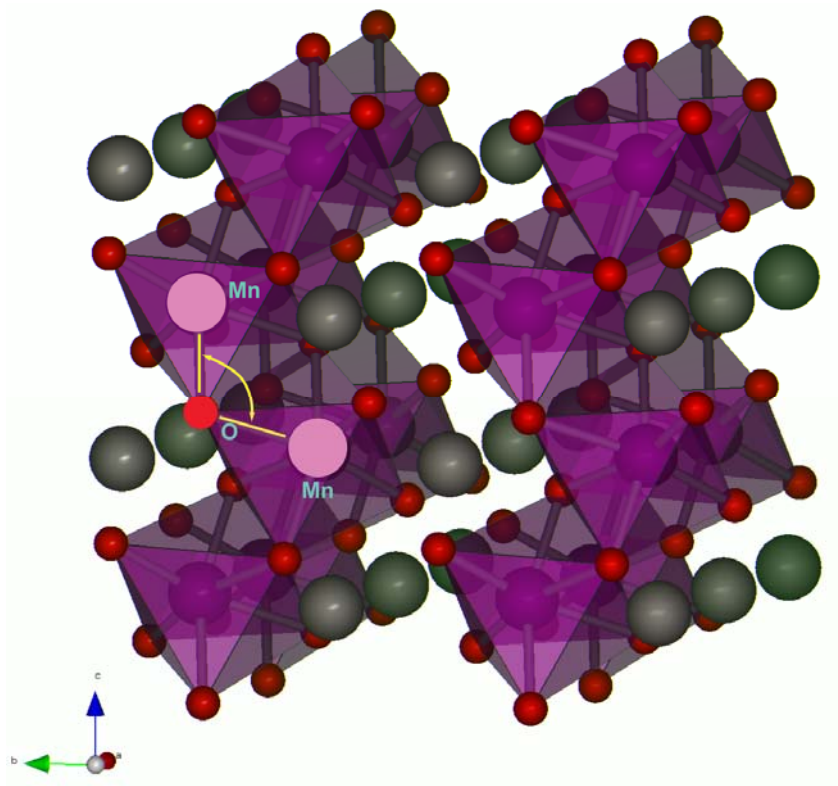
# Spin-wave excitations in the multiferroic antiferromagnet $\text{Mn}_{1-x}\text{Fe}_x\text{WO}_4$ : an experiment using the NCNR Disk Chopper Spectrometer

Summer School on Methods and Applications of Cold and Thermal Neutron  
Spectroscopy  
NIST Center for Neutron Research  
June 19-23, 2011

Yiming Qiu, Feng Ye\*, and John Copley

## Abstract

Time-of-flight neutron spectroscopy is used to measure the spin-wave excitations in multiferroic  $\text{Mn}_{1-x}\text{Fe}_x\text{WO}_4$ . This experiment illustrates the important technique of time-of-flight inelastic neutron scattering. We shall discuss all aspects of the single crystal experiment, from sample alignment and the choice of instrumental setup through to data treatment and interpretation of results.



\*Oak Ridge National Laboratory

## **I. Introduction**

Multiferroics are materials that possess more than one primary ferroic order parameter simultaneously, including ferromagnetism, ferroelectricity, and ferroelasticity. The coupling among the different ferroic orders can lead to important technological applications such as devices that can tune one ferroic property by exploiting a different ferroic order.

The term multiferroic can be expanded to include non-primary order parameters, such as antiferromagnetism, which is the case for  $\text{MnWO}_4$ .  $\text{MnWO}_4$  is a magnetoelectric multiferroic material, exhibiting the coexistence of ferroelectricity and complex magnetic orders. At  $T$  below  $T_{N1}=7.8$  K, the  $\text{Mn}^{2+}$  spins form a collinear antiferromagnetic order. Between  $T_{N1}$  and  $T_{N2}=12$  K, the magnetic order evolves into an incommensurate elliptical spiral configuration accompanied by a spontaneous electric polarization along the crystalline  $b$  axis. When the temperature is further raised between  $T_{N2}$  and  $T_{N3}\approx 13.5$  K, the magnetic structure becomes collinear and incommensurate, and the polarization becomes paraelectric. The phase boundaries can be shifted by doping with Zn or Fe ions at the Mn site. The electric properties are also modified. In the Fe doped  $\text{Mn}_{1-x}\text{Fe}_x\text{WO}_4$ , the low temperature magnetic phase is still the collinear commensurate structure.

To characterize the magnetic interactions that underlie the formation of the spin structures and better understand how the change in exchange couplings affects the evolution between different phases, we study the spin-wave spectra in an Fe-doped single crystal sample.

We use the Disk Chopper Spectrometer at the NIST Center for Neutron Research (NCNR) for this measurement. After reading the background material you should be able to choose an appropriate spectrometer configuration to probe the spin-wave excitations in this system.

The neutron has several properties that enable scattering experiments to measure properties of materials that other techniques can measure with much less precision or not at all. Neutrons with wavelengths on the order of interatomic spacings also possess energies on the same order as those characteristic of phonons and intermolecular interactions; for example, a  $1.8 \text{ \AA}$  neutron has an energy of  $\sim 25 \text{ meV}$  ( $\sim 200 \text{ cm}^{-1}$ ) and speed  $\sim 2200 \text{ ms}^{-1}$ . This means that structural and temporal information can be measured simultaneously.

The reader is reminded that the scattering of neutrons is usually treated as the sum of two parts, known as *coherent* and *incoherent* scattering. To understand why such a separation is performed recall that the strength of the scattering from nuclei of the same element can vary (and generally does vary) with spin and/or isotopic species. Hence when a neutron is scattered by a collection of nuclei the interference between the different scattered waves is normally neither complete nor completely absent. For this reason the *double differential cross section* [ $d^2\sigma/d\Omega d\omega$ ], which describes the probability that neutrons are scattered into solid angle  $d\Omega$  and energy transfer window  $d(\hbar\omega)$ , is normally separated

into two terms. The first term is the coherent part, which contains all of the interference effects such as Bragg scattering and small angle scattering. The second term is the incoherent scattering, which represents the scattering from individual nuclei and is approximately isotropic. For the spin-waves in a Heisenberg model, we are only interested in the coherent part. One can derive the double differential cross section based on linear spin-wave theory which only considers the one magnon cross-section and doesn't take into account the interaction between two or more magnons:

$$\left(\frac{d^2\sigma}{d\Omega dE'}\right)^\pm = r_0^2 \frac{k'}{k} \left\{ \frac{1}{2} g F(\mathbf{Q}) \right\}^2 (1 + \tilde{Q}_z^2) \exp\{-2W(\mathbf{Q})\} \frac{1}{2} S \quad (1)$$

$$\times \frac{(2\pi)^3}{v_0} \sum_{\mathbf{q}, \tau} \left(n_{\mathbf{q}} + \frac{1}{2} \pm \frac{1}{2}\right) \delta(\hbar\omega_{\mathbf{q}} \mp \hbar\omega) \delta(\mathbf{Q} \mp \mathbf{q} - \boldsymbol{\tau}),$$

where + and – correspond to the creation and annihilation of one magnon,  $k$  and  $k'$  are the magnitudes of the initial and final neutron wave vectors,  $r_0=0.54 \times 10^{-14}$  m is a useful unit for magnetic scattering length,  $g$  is the Landé splitting factor,  $F(\mathbf{Q})$  is the magnetic form factor,  $\exp\{-2W(\mathbf{Q})\}$  is the Debye-Waller factor,  $S$  is the spin number,  $v_0$  is the volume of a unit cell,  $\omega_{\mathbf{q}}$  is the magnon energy,  $n_{\mathbf{q}} = [\exp(\hbar\omega_{\mathbf{q}} / k_B T) - 1]^{-1}$ , and  $\mathbf{Q} = \mathbf{k} - \mathbf{k}'$ . Since the above formula contains momentum and energy conservation conditions, inelastic neutron scattering can be used to determine the complete spin-wave spectrum.

What gives rise to the Debye-Waller factor?

Elastic neutron scattering is scattering with no change in neutron energy, i.e. with  $\hbar\omega = 0$ , and inelastic neutron scattering (INS) is scattering with a change in neutron energy, i.e. with  $\hbar\omega \neq 0$ . On the other hand, quasielastic neutron scattering involves the Doppler-like broadening of otherwise elastically scattered neutrons due to reorientational or diffusive motions of atoms in the target material. In this experiment we use neutron scattering to measure INS spectra at very low temperatures and interpret the previously measured data.

We shall first describe the spectrometer as well as matters to be considered in choosing the incident wavelength for this experiment. The next section gives a brief view of the sample and its alignment. We then describe the reduction of the data to obtain the inelastic spectrum. This then sets the scene for the analysis and extraction of the exchange couplings that lead to the spin-wave spectrum.

## II. The spectrometer

This experiment is performed using the Disk Chopper Spectrometer (DCS), which is a so-called “direct geometry” (fixed incident energy) time-of-flight spectrometer. In this type of instrument (figure 1) bursts of monochromatic neutrons strike the sample at equally spaced times. The energies of the scattered neutrons are determined from their arrival times at the detectors, since we know when the pulses were created as well as the distances  $D_{PS}$  from the pulsing device to the sample and  $D_{SD}$  from the sample to the detectors. There are two ways to produce a monochromatic pulsed beam at a steady state neutron source. One method is to use a single crystal to monochromate the white beam and a mechanical “chopper” to pulse it; the other method is to use multiple choppers, such as the seven (!) choppers of the DCS.

A monochromatic pulsed beam of neutrons can in principle be created using two choppers. How does that work? Can you think why more than two choppers might be needed and/or desirable?

Given the initial and final energies of the neutrons,  $E_i$  and  $E_f$ , the energy transfer  $\hbar\omega = E_i - E_f$  is trivially obtained. Knowing the scattering angle  $2\theta$  we can also calculate the magnitude of the momentum transfer to the sample,  $\hbar Q$  :

$$(\hbar Q)^2 = 2m_n \left[ E_i + E_f - 2\sqrt{E_i E_f} \cos 2\theta \right], \quad (2)$$

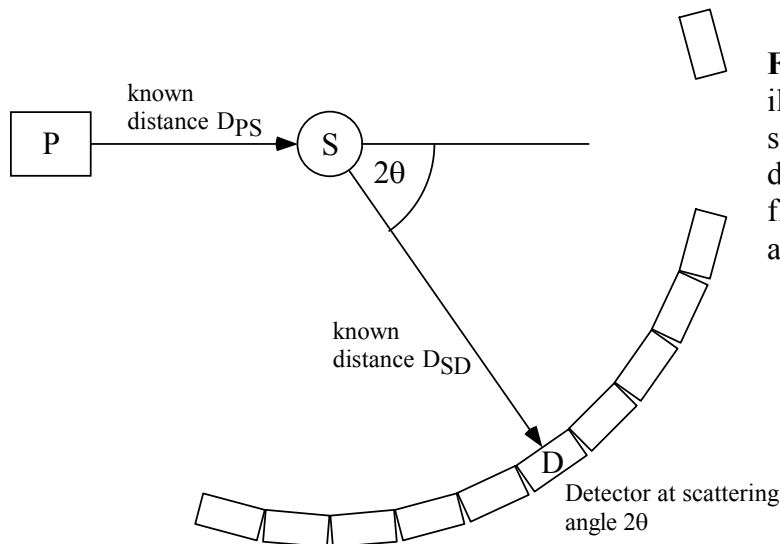


**Figure 1.** A schematic illustration of the scattering geometry for a direct geometry time-of-flight spectrometer such as the DCS.

where  $m_n$  is the mass of the neutron. (This follows from the definition  $\vec{Q} = \vec{k}_i - \vec{k}_f$  and the relationship between the magnitude of a neutron's wave vector,  $k$ , and its energy  $E$ :  $E = \hbar^2 k^2 / 2m_n$ .)

The data acquisition system separately accumulates neutron counts for each of the 913 DCS detectors. Furthermore the time between pulses,  $T$ , is normally divided into 1000 time channels of equal width  $\Delta t = 0.001T$  and each neutron event in a given detector is stored in one of these time channels according to its time of arrival at the detector. Thus the data acquisition system generates a two-dimensional array of counts  $I(i,j)$  as a function of detector index  $i$  and time channel index  $j$ . This array is accumulated in a "histogramming memory" which is resident in the data acquisition computer and reflected to the instrument computer. At the end of each run cycle the array is saved, along with other pertinent information, to the hard disk of the instrument computer.

With the sample environment mounted on the spectrometer, we can control and monitor the temperature remotely. We must also set the incident wavelength, together with a few other parameters such as the "master speed" of the choppers. The choice of wavelength is critical to the experiment and several factors must be considered. These include intensity at the sample (which peaks, remaining roughly constant, between  $\sim 2.5$  and  $\sim 4.5$  Å, see Appendix A), the width of the elastic energy resolution function (which roughly varies as  $1/\lambda^3$ ), the available  $Q$  range (which varies as  $1/\lambda$ ), and concerns about "frame overlap" problems. A related consideration is the available range of energy transfers in sample energy gain (neutron energy loss).

What is the maximum theoretical sample energy gain that can be measured when the incident energy is  $E_i$ , and how long would it take to measure the intensity of neutrons scattered with this change in energy?

### **III. The sample**

For the experiment, a 3.5% doped  $Mn_{1-x}Fe_xWO_4$  single crystal mounted on an aluminum plate is loaded in a liquid helium cryostat. By pumping the liquid helium, a temperature as low as 1.5 K can be achieved.



**Figure 2.** A 3.5% Fe doped  $\text{Mn}_{1-x}\text{Fe}_x\text{WO}_4$  single crystal mounted on an aluminum plate.

Why do we typically use aluminum for sample mounts and containers and cryostat windows?

The single crystal is mounted with the (020) and (102) symmetry directions in the horizontal scattering plane. At the beginning of the experiment, we need to align the crystal using the Bragg peaks available in the scattering plane. The alignment is done by monitoring the intensity of the corresponding detectors that lie in the scattering plane while rotating the sample. A peak intensity is observed when the orientation of the crystal satisfies Bragg's law.

Can you think of a different way to align a single crystal using a time-of-flight instrument?

For this summer school, the data have been collected beforehand. They include measurements at a range of sample rotation angles to cover the spin-wave spectrum in desired crystal symmetry directions, and empty cryostat measurements for background subtraction. To reduce the data we would normally need a detector normalization file obtained using a sample of vanadium which is an incoherent scatterer, but since we are only interested in the spin-wave dispersion, the vanadium measurement is not necessary.

Why do we use vanadium to normalize the data from different detectors? Hint:  $\sigma_{\text{coh}} = 0.02$  barns/atom,  $\sigma_{\text{inc}} = 5.19$  barns/atom.

#### **IV. Data reduction**

In this section we shall indicate some of the more important steps in the data reduction process. We shall go into greater detail in our discussions at the time that the data reduction takes place.

The measured scattering in a sample run includes contributions from the sample itself, from its container and the sample environment, and from the time-independent background. The empty cryostat measurement contains both the scattering from the sample environment and the time-independent background. By subtracting the empty cryostat measurement, we can get rid of the unwanted scattering and background.

Where does the time independent background come from?

Neglecting effects such as self-shielding and multiple scattering the scattering in detector  $i$  and time channel  $j$  may be related to the corresponding double differential cross section  $[d^2\sigma/d\Omega dt]_{ij}$  (note that this is per unit time, not energy) in the following fashion:

$$I(i, j) = \frac{I_{BM}}{\eta_{BM}} \cdot \left[ \frac{d^2\sigma}{d\Omega dt} \right]_{ij} \Delta\Omega \Delta t \cdot N_m \cdot \eta_{ij}, \quad (3)$$

where  $\Delta\Omega$ , the solid angle subtended by detector  $i$ , and  $\Delta t$ , the width of time channel  $j$ , are (for these measurements) independent of  $i$  and  $j$  respectively,  $N_m$  is the number of sample molecules in the beam,  $\eta_{ij}$  is the efficiency of detector  $i$  for neutrons detected in time channel  $j$ , and  $I_{BM}$  and  $\eta_{BM}$  are respectively the counts and the efficiency of the beam monitor (situated upstream of the sample).

Since we are not trying to extract an absolute cross section we can neglect the multiplicative constants in the above equation, but we usually should not ignore the detector efficiency function  $\eta_{ij}$ . Since all of the detectors are to first order identical it is not unreasonable to treat  $\eta_{ij}$  as the product of two terms, a function  $\eta_{i0}$  which represents the efficiency of detector  $i$  for elastically scattered neutrons and a detector-independent function  $f_j$  that describes the energy dependence of the efficiency of the detectors. The correction for differences in detector response, i.e. the determination of  $\eta_{i0}$ , is typically performed using the results of a measurement with a vanadium sample.

The correction of the data for the energy dependence of the efficiency is achieved by calculation, knowing the various factors that affect the probability that a neutron is absorbed within a detector.

What are these factors? Can you write an expression for the efficiency of a detector, assuming its cross section is rectangular?

To improve statistics we sometimes define several detector “groups”, each of which includes detectors within a specified range of angles. The differential cross section  $[d^2\sigma/d\Omega dt]$  for all detectors in a group will be summed and divided by the number of detectors in the group. Having obtained a quantity proportional to  $[d^2\sigma/d\Omega dt]$  we must now compute  $[d^2\sigma/d\Omega d\omega]$  and finally  $S(Q, \omega)$ . Since a neutron’s energy  $E$  is related to its time-of-flight  $t$  over a fixed distance as  $E \propto t^{-2}$ , it follows that  $dE \propto t^{-3} dt$ . Hence

$$\frac{d^2\sigma}{d\Omega d\omega} \propto \frac{d^2\sigma}{d\Omega dE_f} = \left[ \frac{d^2\sigma}{d\Omega dt} \right] \left( \frac{dt}{dE_f} \right) \propto \left[ \frac{d^2\sigma}{d\Omega dt} \right] t^3. \quad (4)$$

To obtain  $S(\mathbf{Q}, \omega)$  we simply divide by  $k_f$  (see eq. 1). Equivalently we multiply by another factor of  $t$  so that  $S(\mathbf{Q}, \omega) \propto I_{ij} t^4$ .

Having reduced the experimental data to the scattering function it is time to interpret the results.

## V. Theory

The spin-wave dispersion curves can be modeled by a general effective Heisenberg Hamiltonian:

$$H = -\sum_{i,j} J_{i,j} \mathbf{S}_i \cdot \mathbf{S}_j - D \sum_i S_{iz}^2, \quad (5)$$

where  $\sum_{i,j}$  is the summation over pairs of spins,  $D$  is the single-ion anisotropy, and  $S_{iz}$  are the spin components along the easy axis. Using the previously determined magnetic structure, the magnetic scattering cross-section can be evaluated as follows:

$$\frac{d^2\sigma}{d\Omega dE} \propto f^2(Q) e^{-2W} \sum_{\alpha\beta} (\delta_{\alpha\beta} - \hat{Q}_\alpha \hat{Q}_\beta) S^{\alpha\beta}(\mathbf{Q}, \omega), \quad (6)$$

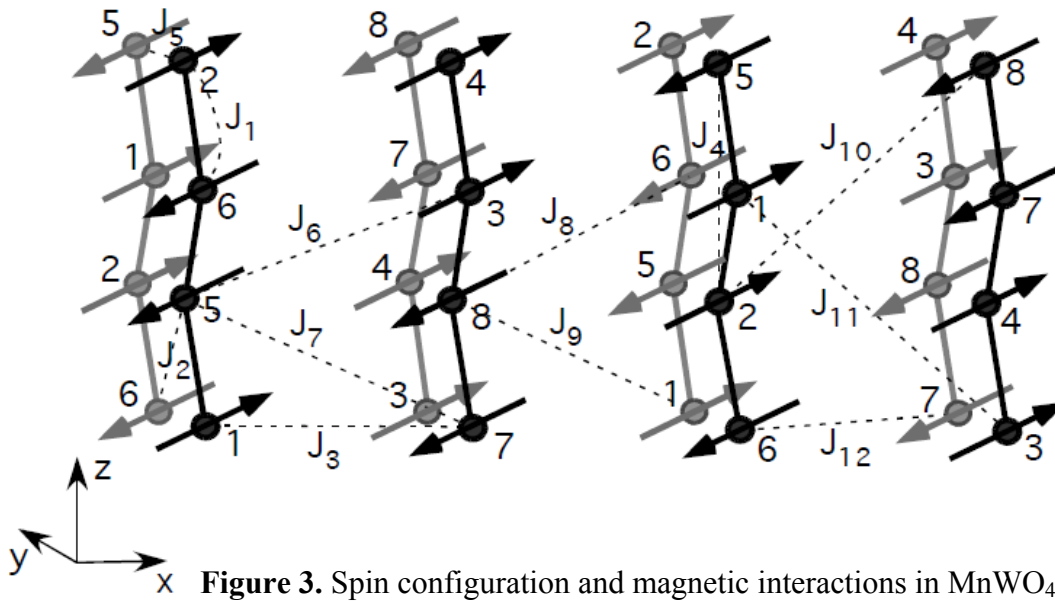
where  $f^2(Q)$  is the magnetic form factor,  $e^{-2W}$  is the Debye-Waller factor as in Eq. (1),  $\hat{Q}_\alpha$  is the  $\alpha$  component of a unit vector in the direction of the wave vector transfer  $\mathbf{Q}$ , and  $S^{\alpha\beta}(\mathbf{Q}, \omega)$  is the response function that describes the spin-spin correlations.

Combining data along all symmetry directions the dispersion relation can be simultaneously modeled using Eq. (5).

## VI. Data analysis

We will first plot the reduced data to show the dispersion curve in the high symmetry directions. After that we will try to fit the dispersion curve with the first nine exchange couplings shown in Fig 3 and the single-ion anisotropy  $D$ .

The calculation of the spin-spin correlation function involves complicated matrix diagonalization and matrix element calculations. An existing spin-wave modeling program will be used to simplify the process.



## VII. Concluding remarks

In the data analysis, we used nine exchange couplings and the anisotropy to fit the spin-wave dispersion. In most cases, linear spin-wave calculations based on nearest and next nearest interactions are enough to characterize a spin-wave spectrum. However, there are systems where quantum fluctuation renders the spin-wave theory invalid, and there are also systems that require considerations of magnon-magnon interactions, which the linear theory doesn't take into account.

The data used in the summer school come from an experiment performed on the DCS by Feng Ye and Jaime Fernandez-Baca. The figures and analysis programs are courtesy of Feng Ye.

## VIII. General references

- G.E. Bacon, "*Neutron Diffraction*", Clarendon Press, Oxford (1975).
- S.W. Lovesey, "*Theory of Neutron Scattering from Condensed Matter, volume 2*", Clarendon Press, Oxford (1984).
- G.L. Squires, "*Introduction to the Theory of Thermal Neutron Scattering*", Cambridge University Press (1978), republished by Dover (1996).

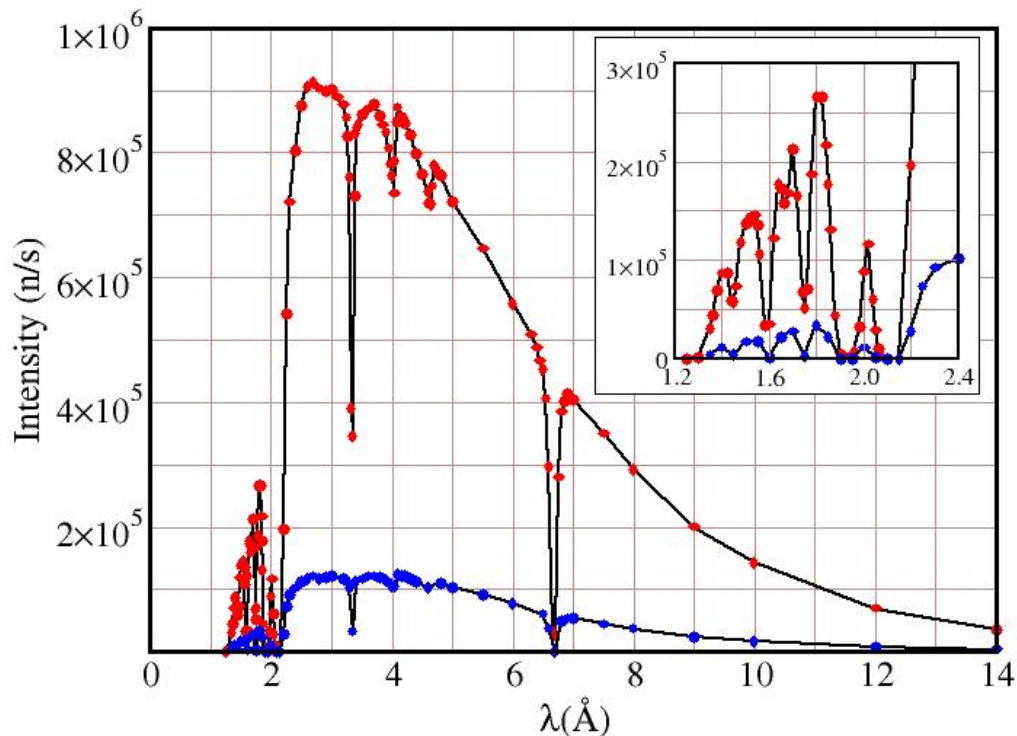
## Appendix A. Principal Characteristics of the Disk Chopper Spectrometer

(<http://www.ncnr.nist.gov/instruments/dcs>)

The white beam from the cold neutron source is cleaned of high energy neutron and gamma ray contamination using an “optical filter”. This is basically a bent guide which ensures that there is no line of sight from the source to points beyond the local shutter. A cooled graphite filter removes short wavelength ( $\sim 0.5 \text{ \AA}$ ) neutrons that remain in the beam, permitting measurements at wavelengths down to roughly  $1.5 \text{ \AA}$ .

A clean, pulsed, monochromatic neutron beam is produced using seven disk choppers. Chopper speeds may be varied from 1200 to 20000 rpm. The pulsing and monochromating choppers have three slots of different widths. In principle this permits three choices of intensity and resolution at a given wavelength and master chopper speed.

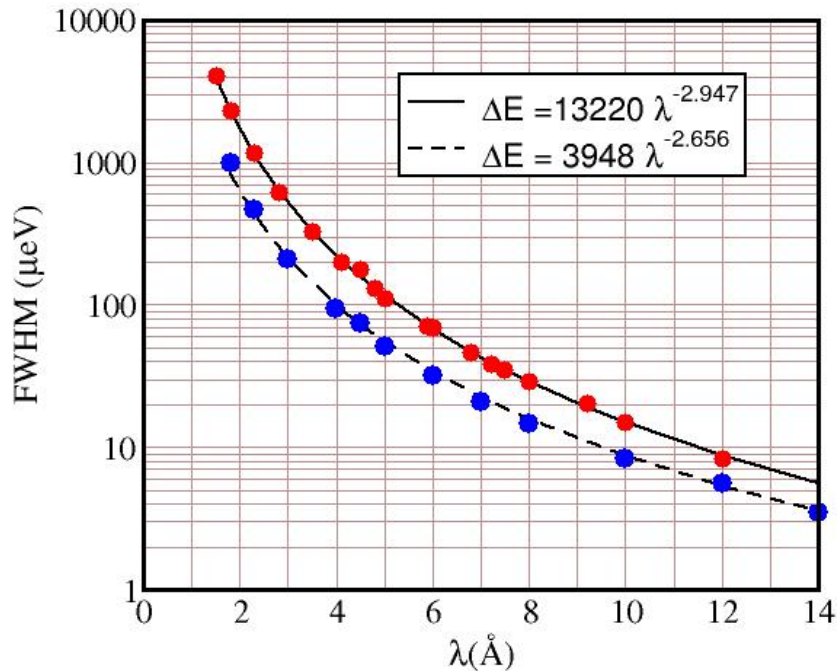
The measured intensity at the sample is reproduced below. Red and blue points (upper and lower plots) correspond to measurements using different chopper slot widths.



Why are there dips in the measured flux at wavelengths near  $3.335$  and  $6.67 \text{ \AA}$ ?  
What's going on around  $1.5$  to  $2 \text{ \AA}$ ?

The resolution of the instrument is approximately triangular and essentially independent of beam height (10 cm) but depends on the width of the beam. Hence samples should ideally be tall and thin rather than short and fat.

The measured elastic energy resolution, for the same choices of chopper slot width as in the intensity plot above, is shown in the figure below. Lines represent fits to the measurements.



An oscillating radial collimator, inside radius 200 mm, outside radius 300 mm, blade separation 2°, is used to reduce the scattering from sample environment structures.

Can you explain how the radial collimator works, and why it is oscillated?

There are 913 six atmosphere <sup>3</sup>He detectors covering an essentially continuous solid angle of ~0.65 steradians and arranged in three banks:

- Middle bank detector scattering angles range from -30° to -5° and from +5° to +140°
- Upper and lower bank angles range from -30° to -10° and from +10° to +140°

The flight distance from sample to detectors is 4010 mm. The flight chamber is purged with argon.

Why is the flight chamber purged with argon?

## Appendix B. Possible Experiments using the Disk Chopper Spectrometer

Phenomena that can be investigated include:

- Translational and rotational diffusion processes, where scattering experiments provide information about time scales, length scales and geometrical constraints; the ability to access a wide range of wave vector transfers, with good energy resolution, is key to the success of such investigations
- Low energy vibrational and magnetic excitations and densities of states
- Tunneling phenomena
- Low Q powder diffraction

Research areas include:

- **Chemistry** --- e.g. clathrates, molecular crystals, fullerenes
- **Polymers** --- bound polymers, glass phenomenon, confinement effects
- **Biological systems** --- protein folding, protein preservation, water dynamics in membranes
- **Physics** --- adsorbate dynamics in mesoporous systems (zeolites and clays) and in confined geometries, metal-hydrogen systems, glasses, magnetic systems
- **Materials** --- negative thermal expansion materials, low conductivity materials, hydration of cement, carbon nanotubes, proton conductors, metal hydrides

## Appendix C. Some useful properties and relationships

### Neutron properties

Mass:	$1.660 \times 10^{-24}$ g
Electric charge:	0
Spin:	$\frac{1}{2}$
Magnetic moment:	-1.913 nuclear magnetons

### Exact relationships

$$\lambda = \frac{h}{mv} \qquad E = \frac{1}{2}mv^2 \qquad k = \frac{2\pi}{\lambda}$$

### Approximate relationships

$$E[\text{meV}] = \frac{81.8}{(\lambda[\text{\AA}])^2}; \quad v[\text{mm}/\mu\text{s}] = \frac{3.956}{\lambda[\text{\AA}]}; \quad E[\text{meV}] = 2.07(k[\text{\AA}^{-1}])^2; \quad 1 \text{ meV} = 8.1 \text{ cm}^{-1}$$

### Appendix D. Spin Incoherence

The strength of the scattering of a neutron by a nucleus, i.e. the neutron scattering length, depends on the spin of the compound nucleus. For an isotope with nuclear spin  $I$  the combined “nucleus + neutron” spin,  $I'$ , has two possible values,  $I^+ = I+1/2$  and  $I^- = I-1/2$ , with which we associate two possible scattering lengths  $b^+$  and  $b^-$ . Each of the possible values of the combined spin has  $2I'+1$  possible spin states, i.e.  $2(I+1/2)+1 = 2I+2$  and  $2(I-1/2)+1 = 2I$  states respectively, for a total of  $4I+2$  spin states.

If the neutron and nuclear spins are randomly orientated, all states are equally probable, and the probabilities of the combined + and - spin states are  $p^+ = (I+1)/(2I+1)$  and  $p^- = I/(2I+1)$  respectively.

The mean scattering length,  $\langle b \rangle$ , and the mean of the scattering length squared,  $\langle b^2 \rangle$ ,

$$\langle b \rangle = p^+ b^+ + p^- b^- \quad \text{and} \quad \langle b^2 \rangle = p^+ (b^+)^2 + p^- (b^-)^2$$

are used to calculate the coherent and incoherent bound cross sections. These cross sections are defined as follows:

$$\sigma_{\text{coh}} = 4\pi \langle b \rangle^2 \quad \text{and} \quad \sigma_{\text{inc}} = 4\pi (\langle b^2 \rangle - \langle b \rangle^2).$$

Working through the numbers for hydrogen and deuterium is instructive. The relevant scattering lengths for hydrogen are  $b^+ = 1.086 \times 10^{-12}$  cm and  $b^- = -4.751 \times 10^{-12}$  cm, whereas the values for deuterium are  $b^+ = 0.951 \times 10^{-12}$  cm and  $b^- = 0.095 \times 10^{-12}$  cm.